Blending of Inputs and Outputs for Modal Velocity Feedback

Manuel Pusch[1] and Daniel Ossmann[1]

Abstract— Dynamical systems like mechanical structures can be effectively damped by applying forces which oppose the velocity measured at the very same location. To apply this principle also to systems with multiple actuators and sensors of different type and at different locations, a novel control approach is presented in this paper. The control approach aims to damp individual modes by a minimum-gain feedback of blended measurement outputs to blended control inputs. To that end, a numerically efficient algorithm is proposed for computing input and output blending vectors which yield the desired isolation of the target mode(s). The effectiveness of the proposed approach is demonstrated by increasing the modal damping of an aeroelastic system.

I. INTRODUCTION

Active control technologies are commonly applied in order to increase the damping of dynamical systems like mechanical structures. To that end, the underlying system needs to be equipped with actuators and sensors, where a larger number in general allows for a better controller performance but complicates controller design. A well established approach to tackle this problem is the principle of identical location of sensors and actuators, referred to as "collocated control" [1] or "direct output feedback" [2]. Therein, each pair of actuators and sensors is commonly augmented with a single-input single-output (SISO) controller, which is subject to be tuned. Considering that, collocated control provides a great robustness with respect to stability, it is recommended whenever possible [1]. A successful application is presented for example in [3], where cockpit vibrations of the Rockwell B-1 Lancer are suppressed by feeding back acceleration measurements to nearby control vanes. Using velocity measurements, it can even be shown that a simple static gain feedback allows increasing the damping of a dynamical system, which is also known as direct velocity feedback (DVF) [4]. The restriction to collocated actuators and sensors, however, limits the applicability of these approaches for active damping. Furthermore, the collocated control loops generally affect not only the Eigenmodes of interest but rather all controllable and observable Eigenmodes of the considered system. As a remedy, [5] proposes to isolate and damp critical Eigenmodes by blending inputs and outputs yielding a static gain feedback controller. In the presented algorithm, denoted as "modal isolation and damping for adaptive aeroservoelastic suppression" (MIDAAS), the input and output blending vectors are computed iteratively since they are interdependent of each other. Avoiding the issue of selecting appropriate initial values, the algorithm proposed in [6] directly yields input

[1]Manuel Pusch and Daniel Ossmann are with the Department of System Dynamics and Control at the German Aerospace Center (DLR), Germany {manuel.pusch,daniel.ossmann}@dlr.de

and output blending vectors maximizing the controllability and observability of the target mode(s) in terms of the $\mathcal{H}_2$ norm. The $\mathcal{H}_2$-optimal blending approach has successfully been applied to different aeroelastic systems with the goal to damp Eigenmodes causing large structural loads, see [7], [8], [9], [10] for more details. The basic idea is to split a multiple-input multiple-output (MIMO) control design problem into a blending vector design problem and a SISO controller design problem, which offers rich insight into the actual controller structure and allows for a dedicated controller tuning.

In this paper, a novel control approach is presented which combines the $\mathcal{H}_2$-optimal blending vector design from [6] and the DVF from [4]. The proposed control approach, denoted as blending-based modal velocity feedback (MVF), is described in Section II and aims to damp an individual mode by a constant feedback of blended measurements to blended control inputs. To that end, input and output blending vectors are derived in Section III, which yield a SISO system with a modal velocity output and a modal force input when applied. Eventually, a numerical example is presented in Section IV, where the proposed modal control approach is successfully applied to a simplified flexible aircraft model.

II. MODAL CONTROL

A. Modal Decomposition

A linear time-invariant (LTI) system with n_u inputs, n_y outputs and n_x states which is physically realizable can be described as

$$G: \quad \begin{bmatrix} \dot{x} \\ y \end{bmatrix} = \left[\begin{array}{c|c} A & B \\ \hline C & D \end{array} \right] \begin{bmatrix} x \\ u \end{bmatrix},$$

where $A \in \mathbb{R}^{n_x \times n_x}, B \in \mathbb{R}^{n_x \times n_u}, C \in \mathbb{R}^{n_y \times n_x}, D \in \mathbb{R}^{n_y \times n_u}$. Assuming that A is diagonalizable, the real Jordan normal form [11] of G can be computed as

$$\tilde{G}: \quad \begin{bmatrix} \dot{\tilde{x}} \\ y \end{bmatrix} = \left[\begin{array}{ccc|c} \tilde{A}_1 & & 0 & \tilde{B}_1 \\ & \ddots & & \vdots \\ 0 & & \tilde{A}_{n_i} & \tilde{B}_{n_i} \\ \hline \tilde{C}_1 & \ldots & \tilde{C}_{n_i} & D \end{array} \right] \begin{bmatrix} \dot{\tilde{x}} \\ u \end{bmatrix}$$

by applying the similarity transformation

$$x = T\tilde{x} = \begin{bmatrix} T_1 & \ldots & T_{n_i} \end{bmatrix} \tilde{x}.$$

For a real eigenvalue p_i with a real eigenvector v_i, the submatrix $T_i = v_i$ and $\tilde{A}_i = p_i$, $\tilde{B}_i = \tilde{b}_i$, $\tilde{C}_i = \tilde{c}_i$ with $i = 1, .., n_i$. For a conjugate complex pole pair $p_i = \Re(p_i) \pm \Im(p_i)$ associated with the conjugate complex eigenvector pair

$v_i = \Re(v_i) \pm \Im(v_i)$, the submatrix $T_i = [\Re(v_i)\ \Im(v_i)]$ and

$$\tilde{A}_i = \begin{bmatrix} \Re(p_i) & \Im(p_i) \\ -\Im(p_i) & \Re(p_i) \end{bmatrix}, \tilde{B}_i = \begin{bmatrix} \Re(\tilde{b}_i)^T \\ -\Im(\tilde{b}_i)^T \end{bmatrix}, \quad (1)$$

$$\tilde{C}_i = \begin{bmatrix} \Re(\tilde{c}_i) & \Im(\tilde{c}_i) \end{bmatrix}.$$

The vectors $\tilde{b}_i$ and $\tilde{c}_i$ are real for real poles and are called pole input and output vectors, respectively. Based on that, the output

$$y = \sum_{i=1}^{n_i} y_i + Du$$

can be described as a superposition of the direct feedthrough Du and the responses of the individual modes

$$\tilde{M}_i: \quad \begin{bmatrix} \dot{\tilde{x}}_i \\ y_i \end{bmatrix} = \begin{bmatrix} \tilde{A}_i & \tilde{B}_i \\ \hline \tilde{C}_i & 0 \end{bmatrix} \begin{bmatrix} \tilde{x}_i \\ u \end{bmatrix}.$$

Hence, a mode $\tilde{M}_i$ is a strictly proper LTI system of first (real pole) or second (conjugate complex pole pair) order and has n_u inputs and n_y outputs.

B. Oscillating Modes

In case of a conjugate complex pole pair $p_i = \Re(p_i) \pm \Im(p_i)$ with $\Im(p_i) \neq 0$, the mode $\tilde{M}_i$ describes a harmonic oscillator with a natural frequency $\omega_n = |p_i|$ and a relative damping $\zeta = -\Re(p_i)/\omega_n$. This motivates the description of $\tilde{M}_i$ in physical coordinates where the modal deflection ξ and its derivative, the modal velocity $\dot{\xi}$, are the two state variables. Given the mode $\tilde{M}_i$ in real Jordan normal form (1), its physical realization is

$$M_i: \quad \begin{bmatrix} \dot{\xi} \\ \ddot{\xi} \\ y_i \end{bmatrix} = \begin{bmatrix} 0 & 1 & b_1^T \\ -\omega_n^2 & -2\zeta\omega_n & b_2^T \\ \hline c_1 & c_2 & 0 \end{bmatrix} \begin{bmatrix} \xi \\ \dot{\xi} \\ u \end{bmatrix}, \quad (2)$$

which is obtained by the similarity transformation $\tilde{x}_i = \tilde{T}_i [\xi\ \dot{\xi}]^T$. While M_i features a unique system matrix

$$\tilde{T}_i^{-1} \tilde{A}_i \tilde{T}_i = \begin{bmatrix} 0 & 1 \\ -\omega_n^2 & -2\zeta\omega_n \end{bmatrix},$$

the transformation matrix $\tilde{T}_i$ and the vectors $b_1 \in \mathbb{R}^{n_u}$, $b_2 \in \mathbb{R}^{n_u}$, $c_1 \in \mathbb{R}^{n_y}$ and $c_2 \in \mathbb{R}^{n_y}$ are not unique. To obtain all possible physical realizations, $\tilde{T}_i$ can be parametrized as

$$\tilde{T}_i(\alpha, \phi) = \alpha \begin{bmatrix} -\Re(p_i)\sin\phi + \Im(p_i)\cos\phi & \sin\phi \\ -\Im(p_i)\sin\phi - \Re(p_i)\cos\phi & \cos\phi \end{bmatrix}, \quad (3)$$

where $\alpha \in \mathbb{R} \setminus \{0\}$ and $\phi \in \mathbb{R}$, see [11] for more details. Applying the similarity transformation (3) on Equation (1) hence yields

$$\begin{bmatrix} b_1^T \\ b_2^T \end{bmatrix} = \begin{bmatrix} b_1^T(\alpha, \phi) \\ b_2^T(\alpha, \phi) \end{bmatrix} = \tilde{T}_i^{-1}(\alpha, \phi) \begin{bmatrix} \Re(\tilde{b}_i)^T \\ -\Im(\tilde{b}_i)^T \end{bmatrix} \quad (4)$$

and

$$\begin{aligned} \begin{bmatrix} c_1 & c_2 \end{bmatrix} &= \begin{bmatrix} c_1(\alpha, \phi) & c_2(\alpha, \phi) \end{bmatrix} \\ &= \begin{bmatrix} \Re(\tilde{c}_i) & \Im(\tilde{c}_i) \end{bmatrix} \tilde{T}_i(\alpha, \phi). \end{aligned} \quad (5)$$

Note that a special physical realization for single input systems ($n_u = 1$) is the *controllable canonical form*, which is derived by setting $\alpha = -|\tilde{b}_i|$ and $\phi = \arg(-j\tilde{b}_i)$ yielding $[b_1\ b_2] = [0\ 1]$.

C. Direct Velocity Feedback

In order to increase the damping of dynamical systems like mechanical structures, numerous control approaches have been proposed, see for example [1] for a comprehensive overview. A very intuitive concept is to generate a force input proportional to the velocity measured at the very same location (collocation), which is known as DVF [4]. Considering an individual (oscillating) mode M_i, this requires a special form of its physical realization (2) featuring $c_2 = \beta b_2 \neq 0, \beta \in \mathbb{R}_{\geq 0}$ and $c_1 = b_1 = 0$, which yields the differential equation

$$\ddot{\xi} + 2\zeta\omega_n\dot{\xi} + \omega_n^2\xi = b_2^T u, \ \ y_i = c_2\dot{\xi} = \beta b_2\dot{\xi}. \quad (6)$$

Closing the loop with the feedback matrix $\Lambda \in \mathbb{R}^{n_u \times n_y}$ by setting

$$u = -\Lambda y_i = -\Lambda c_2\dot{\xi}_i = -\Lambda\beta b_2\dot{\xi}_i$$

changes Equation (6) to

$$\ddot{\xi} + \left(2\zeta\omega_n + \beta b_2^T\Lambda b_2\right)\dot{\xi} + \omega_n^2\xi = 0. \quad (7)$$

This means that the relative damping of M_i is changed by $\Delta\zeta = \beta b_2^T\Lambda b_2/(2\omega_n)$ while its natural frequency ω_n remains unchanged. To ensure that damping is rather increased but not decreased, Λ needs to be positive definite [1]. Note, however, that this only holds in general if actuators and sensors are collocated (i.e., $c_2 = \beta b_2$), which certainly limits the application of the DVF approach. Furthermore, the DVF approach may also be applied to higher order systems [4], where all controllable and observable modes are commonly affected by the derived feedback controller. Hence, DVF generally does not allow damping individual modes without affecting others.

D. Blending-based Modal Velocity Feedback

Based on DVF, a novel control approach is presented herein for damping individual modes using multiple actuators and sensors of different type and at different locations. The control approach, denoted as blending-based MVF, aims to control individual modes by means of a constant feedback of blended measurement outputs to blended control inputs. The resulting tunable feedback loops are dedicated to individual modes, whereas in the DVF approach, they are dedicated to individual pairs of collocated sensors and actuators.

To begin with, the idea is to blend the measurement outputs such that the resulting virtual measurement signal $v_y = k_y^T y$ represents the modal velocity $\dot{\xi}$ of the mode to be controlled. Similarly, a virtual control input v_u is generated which is distributed to the actual control inputs $u = k_u v_u$ in a way that enables an explicit excitation of the target mode. In other words, by means of the input and output blending vectors $k_u \in \mathbb{R}^{n_u}$ and $k_y \in \mathbb{R}^{n_y}$, the target mode is isolated yielding Equation (6) with a single input and

a single output, whereby it can be directly damped by a single static feedback gain $\lambda \in \mathbb{R}$. Certainly, this requires a sufficient controllability and observability of the target mode (given by the actual actuator and sensor configuration), which is assumed to be the case here. The resulting feedback
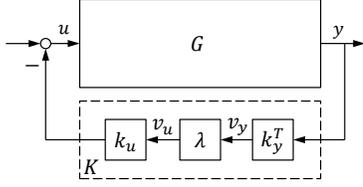

Fig. 1.   Closed-loop interconnection of plant G with controller K.

interconnection is depicted in Figure 1, where the static gain feedback controller

$$K = \lambda k_u k_y^T$$

is encircled with a dashed line. In order to balance between common control design criteria like damping increase, robustness margins or saturation limitations, the controller K can easily be tuned by adjusting the feedback gain λ accordingly. In case it is desired to damp multiple modes, it is proposed to repeat the described control design procedure for each mode to be controlled and superimpose the respective control commands. Note that the modal velocity may also be reconstructed using observer-based methods, see [12] for more details. This, however, typically results in controllers of an increased order since the included observers commonly have the same order as the underlying plant models [12].

III. BLENDING VECTOR DESIGN

A. Problem Formulation

Applying the input and output blending vectors k_u and k_y to an individual mode M_i defined in Equation (2) yields

$$k_y^T M_i k_u : \quad \begin{bmatrix} \dot{\xi} \\ \ddot{\xi} \\ \hline v_y \end{bmatrix} = \begin{bmatrix} 0 & 1 & b_1^T k_u \\ -\omega_n^2 & -2\zeta\omega_n & b_2^T k_u \\ \hline k_y^T c_1 & k_y^T c_2 & 0 \end{bmatrix} \begin{bmatrix} \xi \\ \dot{\xi} \\ \hline v_u \end{bmatrix}.$$

In order to allow for the blending-based MVF described in Section II-D, the blending vectors k_u and k_y need to be designed such that $b_1^T k_u = k_y^T c_1 = 0$. This means that the virtual control input v_u becomes a pure modal force input while the virtual measurement output v_y represents the modal velocity $\dot{\xi}$ and hence, DVF can be applied. Besides, it is desired to find blending vectors which allow increasing the relative damping by $\Delta\zeta$ with a minimum feedback gain λ. Small feedback gains in general imply small control inputs and high robustness margins, see also [12] for more details. Similar to the DVF loop in Equation (7), the MVF loop with blended inputs and outputs is given as

$$\ddot{\xi} + \left(2\zeta\omega_n + \lambda k_y^T c_2 b_2^T k_u\right)\dot{\xi} + \omega_n^2 \xi = 0,$$

where the change in relative damping $\Delta\zeta = \lambda k_y^T c_2 b_2^T k_u / (2\omega_n)$. For a fixed $\Delta\zeta > 0$, $|\lambda|$ becomes minimal when $|k_y^T c_2 b_2^T k_u|$ is maximal since the natural

frequency ω_n does not change. Summing up, the blending vector design problem for MVF can be formulated as

$$\begin{aligned} \underset{k_u \in \mathbb{R}^{n_u}, k_y \in \mathbb{R}^{n_y}}{\text{maximize}} \quad & \left| k_y^T c_2 b_2^T k_u \right| \\ \text{subject to} \quad & \|k_u\|_2 = 1 \\ & \|k_y\|_2 = 1 \\ & b_1^T k_u = 0 \\ & c_1^T k_y = 0, \end{aligned} \tag{8}$$

where the length of the blending vectors is restricted to one to avoid an undesired scaling of the optimization problem. Furthermore, the two constraints $b_1^T k_u = k_y^T c_1 = 0$ enforce that the transfer function of the blended mode is given in the form

$$k_y^T M_i k_u = k_y^T c_2 b_2^T k_u \frac{s}{s + 2\zeta\omega_n s + \omega_n^2}, \tag{9}$$

where s denotes the Laplace variable. From Equation (9), it can be seen that blending vectors which maximize $|k_y^T c_2 b_2^T k_u|$ also maximize the $\mathcal{H}_2$ norm $\left\| k_y^T M_i k_u \right\|_{\mathcal{H}_2}$, considering the constraints from Equation (8). In this respect, the derived blending vectors can be considered as $\mathcal{H}_2$-optimal under the side constraints enabling MVF. In case MVF is not enforced, corresponding $\mathcal{H}_2$-optimal blending vectors can be computed according to [7], where therein, a static gain feedback in general does not yield a pure damping increase.

B. Blending Vector Computation

In the optimization problem (8), the constraints $b_1^T k_u = 0$ and $c_1^T k_y = 0$ enforce the optimal input and output blending vectors to lie in the null space of b_1^T and c_1^T, respectively. This means, the original optimization variables k_u and k_y can be substituted by

$$k_u = N_u \hat{k}_u \tag{10}$$
$$k_y = N_y \hat{k}_y , \tag{11}$$

where N_u and N_y denote an orthonormal basis of the null space of b_1^T and c_1^T. Since N_u and N_y act as unitary linear transformations preserving the inner product, k_u and k_y have the same length as $\hat{k}_u$ and $\hat{k}_y$. Hence, the optimization problem (8) can be reformulated as

$$\begin{aligned} \underset{\hat{k}_u, \hat{k}_y}{\text{maximize}} \quad & \left| \hat{k}_y^T Q(\phi) \hat{k}_u \right| \\ \text{subject to} \quad & \left\| \hat{k}_u \right\|_2 = 1 \\ & \left\| \hat{k}_y \right\|_2 = 1, \end{aligned} \tag{12}$$

where

$$Q(\phi) = N_y^T c_2 b_2^T N_u. \tag{13}$$

Recall that according to Equations (4) and (5), the vectors b_1, b_2 and c_1, c_2 are computed by means of a similarity transformation and depend on the parameters α and ϕ. Considering Equation (13), this means that each of the given variables depends on α and ϕ, where α actually cancels out, i.e., $Q(\alpha, \phi) = Q(\phi)$. From Equation (12), it can be seen that

the actual goal is to find unit vectors $\hat{k}_u$ and $\hat{k}_y$ which yield a maximum absolute value when multiplied with $Q(\phi)$ from the right- and left-hand side, respectively. This is equivalent to finding the right and left singular vectors associated to the largest singular value of $Q(\phi)$. Hence, an equivalent unconstrained optimization problem can be formulated as

$$\phi^* = \arg\max_{\phi \in \mathbb{R}} \|Q(\phi)\|_2, \qquad (14)$$

where $\|Q(\phi)\|_2$ is nothing but the largest singular value of $Q(\phi)$. Note that due to the given periodicity of $\tilde{Q}(\phi)$, the optimization variable ϕ may be restricted to an interval of size π, for instance $\phi \in [0, \pi[$. Solving the optimization problem (14), the optimal blending vectors $k_u^* = N_u \hat{k}_u^*$ and $k_y^* = N_y \hat{k}_u^*$ can be directly derived by means of a singular value decomposition (SVD) of

$$Q(\phi^*) = U \Sigma V^T = \begin{bmatrix} \hat{k}_y^* & \bullet \end{bmatrix} \begin{bmatrix} \sigma^* & 0 \\ 0 & \bullet \end{bmatrix} \begin{bmatrix} \hat{k}_u^* & \bullet \end{bmatrix}^T, \quad (15)$$

where the placeholder $\bullet$ denotes a matrix of adequate size. In Equation (15), the rectangular diagonal matrix $\Sigma \in \mathbb{R}^{(n_y-1)\times(n_u-1)}$ lists the singular values of $Q(\phi^*)$ in descending order on its diagonal. The largest singular value is $\sigma^* = \|Q(\phi^*)\|_2 \in \mathbb{R}_{\geq 0}$, which is associated to the right and left singular vector $\hat{k}_u^*$ and $\hat{k}_y^*$, respectively. Note that $\hat{k}_u^*$ as well as $\hat{k}_y^*$ feature a length of one since both $U \in \mathbb{R}^{(n_y-1)\times(n_y-1)}$ and $V \in \mathbb{R}^{(n_u-1)\times(n_u-1)}$ are orthogonal matrices.

C. Mode Decoupling

So far, input and output blending vectors are derived which yield a minimum static feedback gain for damping the targeted mode. For mode decoupling, however, it is additionally desired that feeding back the blended outputs to the blended inputs prevents an excitation of the residual modes as good as possible. This can be achieved by enforcing the input and output blending vectors to be orthogonal on the respective residual modes, or more specifically on its pole input and output vectors $\tilde{b}_i$ and $\tilde{c}_i$, see Section II for more details. For a complex-valued pole vector, this means that orthogonality is enforced on both the real and imaginary part. Collecting the real and imaginary parts of the respective pole input and output vectors as column vectors in the matrices P_u and P_y, the original optimization problem (8) can be augmented as

$$
\begin{aligned}
\underset{k_u \in \mathbb{R}^{n_u}, k_y \in \mathbb{R}^{n_y}}{\text{maximize}} \quad & \left| k_y^T c_2 b_2^T k_u \right| \\
\text{subject to} \quad & \|k_u\|_2 = 1 \\
& \|k_y\|_2 = 1 \\
& b_1^T k_u = 0 \\
& c_1^T k_y = 0 \\
& P_u^T k_u = 0 \\
& P_y^T k_y = 0,
\end{aligned}
\qquad (16)
$$

where the constraints $P_u^T k_u = 0$ and $P_y^T k_y = 0$ enforce the desired mode decoupling. In order to solve the optimization problem (16), the same procedure as in Section III-B is applied. The only difference is that the matrices N_u and N_y are adapted such that they represent an orthonormal basis of the null space of $[b_1 \; P_u]^T$ and $[c_1 \; P_y]^T$, respectively. If one of the null spaces is empty, the augmented optimization problem (16) is infeasible. This also implies that for a finite number of inputs and outputs, the number of residual modes which can be made uncontrollable or unobservable is limited. Note, however, that for mode decoupling it may be sufficient to make the respective residual modes either uncontrollable or unobservable but not both.

Alternatively, mode decoupling may also be achieved using dynamic filtering, where the target mode needs to be well separated in frequency from the rest of the system. In that case, it is proposed to first band-pass filter the measurement signals to emphasize the response of the target mode. Based on the plant augmented with the band-pass filters, the blending vectors for MVF are then designed as described in Section III-B. Note that the band-pass filters introduce additional tuning parameters and result in controller which is not static.

IV. NUMERICAL EXAMPLE

To demonstrate the effectiveness of the proposed control approach, it is applied to a flexible aircraft with lightly damped modes. For replicability reasons, a low-order approximation of the high-order aeroelastic model is used in this paper. Thereby, the numerical values of the model as well as the resulting controller can be provided herein.

A. System Description

The example given in this paper is based on an aeroelastic model of a large transport aircraft with distributed flaps and measurements taken from [7]. The model used represents only the three most dominating modes in terms of wing bending, where the corresponding properties are summarized in Table I. The underlying state space matrices are provided in the Appendix, with the system featuring four control inputs and eight measurement outputs which are certainly not collocated. The four control inputs are symmetric deflections commands for three pairs of trailing edge flaps on the wing and one pair of elevators. The measurement outputs are four vertical acceleration and four rotational rate sensors placed on the wings of the aircraft.

TABLE I
MODES M_i IN THE FREQUENCY RANGE OF INTEREST.

i	natural frequency ω_n	relative damping ζ
1	$1.6\,\text{rad/s}$	0.42
2	$10.9\,\text{rad/s}$	0.12
3	$18.4\,\text{rad/s}$	0.03

B. Blending-based Modal Velocity Feedback Controller Design

In order to reduce structural loads of the aircraft, the control objective herein is to increase the damping of mode 2 and 3. To that end, the inputs and outputs of the underlying system are blended to isolate both modes so that a minimum

gain MVF is enabled. For comparison reasons, the blending vector design is carried out with and without explicit mode decoupling constraints.

In a first step, a pair of blending vectors is designed for each of the two modes without considering any mode decoupling constraints. The underlying optimization problem is described in Equation (8) and solved according to Equation (12). Normalizing the corresponding objective function $\|Q(\phi)\|_2$ by the constant factor $2\sqrt{\omega_n\zeta}\,\|M_i\|_{\mathcal{H}_2}$ yields the blending efficiency

$$\eta(\phi) = \frac{\left\|k_y(\phi)^T M_i k_u(\phi)\right\|_{\mathcal{H}_2}}{\|M_i\|_{\mathcal{H}_2}} = \frac{\|Q(\phi)\|_2}{2\sqrt{\omega_n\zeta}\,\|M_i\|_{\mathcal{H}_2}}, \quad (17)$$

where the vectors $k_u(\phi)$ and $k_y(\phi)$ are the right and left singular vectors associated to the largest singular value of $Q(\phi)$. The blending efficiency $\eta \in [0\ 1]$ is originally introduced in [7] as a modal controllability and observability measure, where $\eta = 0$ indicates that the mode can not be controlled at all. Herein, however, it is more related to the feedback gain λ required to increase modal damping as described in Section III-A. In Figure 2, η is plotted over ϕ for mode 2 (——) and mode 3 (·····), where it can be seen that the respective maxima can easily be found using some global optimization algorithm. Blending the inputs and outputs with the obtained blending vectors results in a system with two virtual control inputs and two virtual control outputs, which is plotted in Figure 3. It has to be acknowledged that all three modes can be controlled and observed by the blended inputs and outputs instead of being dedicated to the respective target modes as desired.
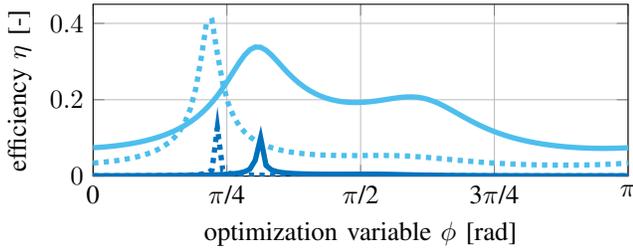

Fig. 2. Comparison of efficiency factors for mode 2 and mode 3 with (——, ·····) and without (——, ·····) mode decoupling constraints, respectively.

Hence, in a second step, blending vectors are designed taking into account also mode decoupling constraints. In order to leave mode 1 unaffected, it needs to be either uncontrollable by the blended inputs or unobservable by the blended outputs. For the latter, the maximum achievable blending efficiency η is considerably larger because the number of independent measurement outputs is much larger than the number of control inputs. Thus, mode 1 is only made unobservable by enforcing the corresponding output blending vectors $k_{y,2}$ and $k_{y,3}$ to be orthogonal on its pole output vector $\tilde{c}_1$. In other words, an explicit decoupling from mode 1 is achieved with the constraints $\tilde{c}_1^T k_{y,2} = 0$ and $\tilde{c}_1^T k_{y,3} = 0$. Additionally, an independent control of mode 2
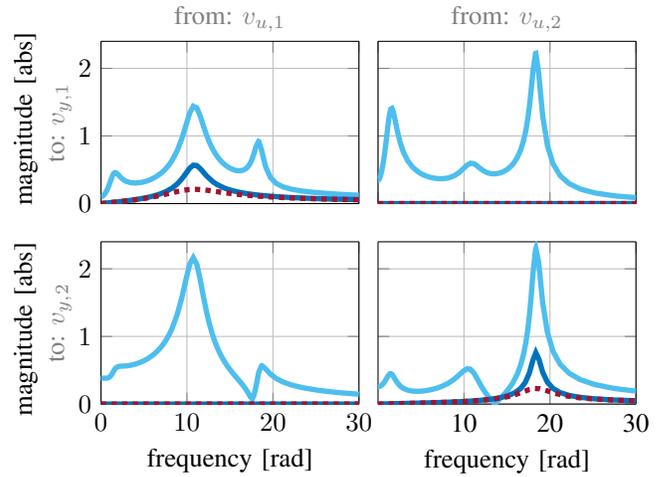

Fig. 3. Comparison of frequency response from blended inputs to blended outputs with (——) and without (——) mode decoupling constraints together with the closed-loop response (·····).

and mode 3 is desired. This can be achieved by enforcing the input and output blending vectors of one mode to be orthogonal on the pole input and output vectors of the other mode. The corresponding constraints for input blending are $\tilde{b}_3^T k_{u,2} = 0$ and $\tilde{b}_2^T k_{u,3} = 0$, where $\tilde{b}_2$ and $\tilde{b}_3$ are the pole input vectors of mode 2 and mode 3, respectively. Similarly, the output blending vectors are constrained by $\tilde{c}_3^T k_{y,2} = 0$ and $\tilde{c}_2^T k_{y,3} = 0$ with $\tilde{c}_2$ and $\tilde{c}_3$ denoting the respective pole output vectors. Summing up, the matrices of the mode decoupling constraints in Equation (16) are given for the output side as

$$P_{y,2} = \begin{bmatrix} \Re(\tilde{c}_1) & \Im(\tilde{c}_1) & \Re(\tilde{c}_3) & \Im(\tilde{c}_3) \end{bmatrix},$$
$$P_{y,3} = \begin{bmatrix} \Re(\tilde{c}_1) & \Im(\tilde{c}_1) & \Re(\tilde{c}_2) & \Im(\tilde{c}_2) \end{bmatrix},$$

and for the input side as

$$P_{u,2} = \begin{bmatrix} \Re(\tilde{b}_3) & \Im(\tilde{b}_3) \end{bmatrix},$$
$$P_{u,3} = \begin{bmatrix} \Re(\tilde{b}_2) & \Im(\tilde{b}_2) \end{bmatrix}.$$

Solving the augmented optimization problem (16), the optimal blending vectors are computed according to Equation (15) as

$$k_{y,2} = \begin{bmatrix} 0.477 \\ 0.031 \\ -0.224 \\ -0.407 \\ -0.238 \\ -0.221 \\ 0.671 \\ 0.018 \end{bmatrix}, \ k_{y,3} = \begin{bmatrix} -0.317 \\ 0.263 \\ 0.054 \\ 0.018 \\ 0.164 \\ 0.244 \\ -0.777 \\ 0.37 \end{bmatrix},$$

and

$$k_{u,2} = \begin{bmatrix} 0.056 \\ 0.489 \\ 0.85 \\ -0.189 \end{bmatrix}, \ k_{u,3} = \begin{bmatrix} -0.558 \\ -0.036 \\ 0.669 \\ 0.489 \end{bmatrix}.$$

The successful decoupling of modes can be seen in Figure 3 (——), where the modes to be controlled are clearly emphasized in the respective channels while no other modes are

visible. It needs to be mentioned, however, that the enforced mode decoupling leads to a degradation of the maximum achievable blending efficiency η as it is recognizable in Figure 2. This can also be seen in Figure 3, where the resonance peaks of the target modes are reduced when considering mode decoupling. Taken as a whole, this trade-off is acceptable as sufficient controllability and observability of the target modes (e.g. in terms of the $\mathcal{H}_2$ norm [7]) are still given.

In a third and final step, the control gains λ need to be determined for both modes to be controlled. This additional degrees of freedom allow to adjust control performance such that common constraints like actuator limitations or robustness criteria are met, where $\lambda = 3$ is chosen here for both modes. Closing the control loop shifts the poles as given in Figure 4, where it can be seen that the relative damping is increased by a factor of 2.7 and 3.8 for mode 2 and mode 3, respectively. On the contrary, mode 1 is not affected as an invariant zero is placed at its pole location when considering an explicit mode decoupling. Furthermore, the increased modal damping is also visible in Figure 3, where the resonance peaks are clearly reduced. This proves the applicability of the proposed modal control approach.
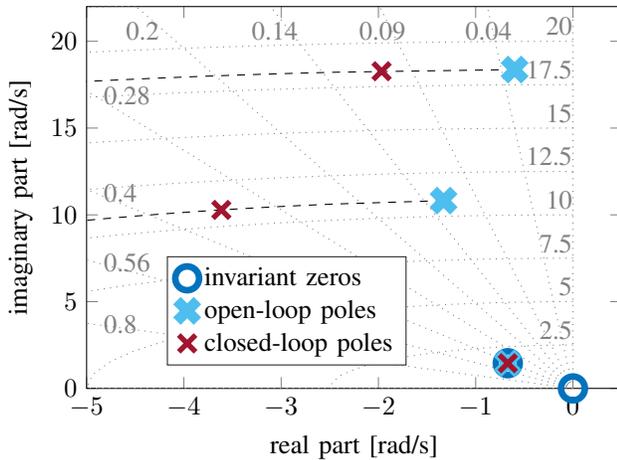

Fig. 4. Invariant zeros and poles of the open- and closed-loop system with blended inputs and outputs together with the illustration of the root locus (- - -).

V. Conclusion

The novel control approach presented in this paper is denoted as blending-based modal velocity feedback (MVF) and aims to damp individual modes of multiple-input multiple-output (MIMO) systems. The approach splits the challenge of designing a suitable MIMO controller into the blending of inputs and outputs and a subsequent tuning of a constant feedback gain. The goal for designing the corresponding blending vectors is to isolate the target mode(s) in a way such that a minimum feedback gain is required for a certain damping increase. A numerically efficient algorithm is derived which allows a joint computation of the interdependent input and output blending vectors by solving an unconstrained

optimization problem in a single variable. The successful application of the proposed control approach to an aeroelastic system proves its effectiveness, where two modes are isolated and actively damped.

Appendix

State Space Matrices of the Numerical Example

The state space matrices of the linear time-invariant (LTI) system used in Section IV are given in a real Jordan normal form as

$$A = \begin{bmatrix} -0.67 & -1.45 & 0 & 0 & 0 & 0 \\ 1.45 & -0.67 & 0 & 0 & 0 & 0 \\ 0 & 0 & -1.33 & -10.82 & 0 & 0 \\ 0 & 0 & 10.82 & -1.33 & 0 & 0 \\ 0 & 0 & 0 & 0 & -0.6 & -18.37 \\ 0 & 0 & 0 & 0 & 18.37 & -0.6 \end{bmatrix}$$

$$B = \begin{bmatrix} 0.01 & -0.01 & -0.01 & -0.18 \\ -0.21 & -0.2 & -0.09 & -2.63 \\ 0.91 & 1.56 & 1.67 & -1.13 \\ -1.06 & -1.32 & -1.08 & 0.17 \\ 0.44 & 0.04 & -0.6 & -2.46 \\ -0.26 & 0.11 & 0.64 & 3.08 \end{bmatrix}$$

$$C = \begin{bmatrix} 0.04 & 0.73 & 0.03 & 0 & -0.02 & 0 \\ 0 & 0.63 & -0.43 & 0.07 & -1.06 & -0.09 \\ -0.09 & 0.44 & -1.36 & 0.06 & -0.56 & -0.12 \\ -0.13 & 0.34 & -1.79 & -0.05 & 0.1 & 0.03 \\ -0.21 & 0.03 & 0.03 & 0.01 & -0.05 & -0.13 \\ -0.23 & -0.04 & -0.3 & -0.03 & -0.72 & -0.21 \\ -0.28 & -0.19 & -1.01 & -0.5 & -0.32 & -0.15 \\ -0.29 & -0.29 & -1.32 & -1.09 & 0.07 & 0.64 \end{bmatrix}$$

$$D = \begin{bmatrix} 0 \end{bmatrix}.$$

References

[1] André Preumont. *Vibration control of active structures*, volume 2. Springer, 1997.

[2] Leonard Meirovitch. *Dynamics and control of structures*. John Wiley & Sons, 1990.

[3] John H. Wykes, Christopher J. Borland, Martin J. Klepl, and Cary J. MacMiller. Design and development of a structural mode control system. *NASA/CR*, 143846, 1977.

[4] Mark J. Balas. Direct velocity feedback control of large space structures. *Journal of Guidance, Control, and Dynamics*, 2(3):252–253, 1979.

[5] B. Danowsky, P. Thompson, D.-C. Lee, and M. Brenner. Modal isolation and damping for adaptive aeroservoelastic suppression. In *AIAA Atmospheric Flight Mechanics Conference*, Boston, MA, USA, 2013.

[6] Manuel Pusch and Daniel Ossmann. $\mathcal{H}_2$-optimal Blending of Inputs and Outputs for Modal Control. *Submitted to Transaction of Control System Technology*, 2018.

[7] Manuel Pusch. Aeroelastic mode control using $\mathcal{H}_2$-optimal blends for inputs and outputs. In *AIAA Guidance, Navigation, and Control Conference*, Orlando, FL, USA, 2018.

[8] Manuel Pusch, Daniel Ossmann, Johannes Dillinger, Thiemo M Kier, Martin Tang, and Jannis Lübker. Aeroelastic modeling and control of an experimental flexible wing. In *AIAA Guidance, Navigation, and Control Conference*, San Diego, CA, USA, 2019.

[9] Manuel Pusch, Daniel Ossmann, and Tamás Luspay. Model-based robust control design for a highly felxible flutter demonstrator. *Submitted to Aerospace Open Access Journal*, 2019.

[10] Tamás Luspay, Tamás Baár, Dániel Teubl, Bálint Vanek, Daniel Ossmann, Matthias Wüstenhagen, Manuel Pusch, Thiemo M. Kier, Sergio Waitman, Andrea Ianelli, Andres Marcos, and Mark Lowenberg. Flight control design for a highly flexible flutter demonstrator. In *AIAA Atmospheric Flight Mechanics Conference*, San Diego, CA, USA, 2019.

[11] Thomas Kailath. *Linear systems*, volume 156. Prentice-Hall Englewood Cliffs, NJ, 1980.

[12] Sigurd Skogestad and Ian Postlethwaite. *Multivariable feedback control: analysis and design*, volume 2. Wiley New York, 2007.